Device

Article

Moon photovoltaics utilizing lunar regolith and halide perovskites

Graphical abstract

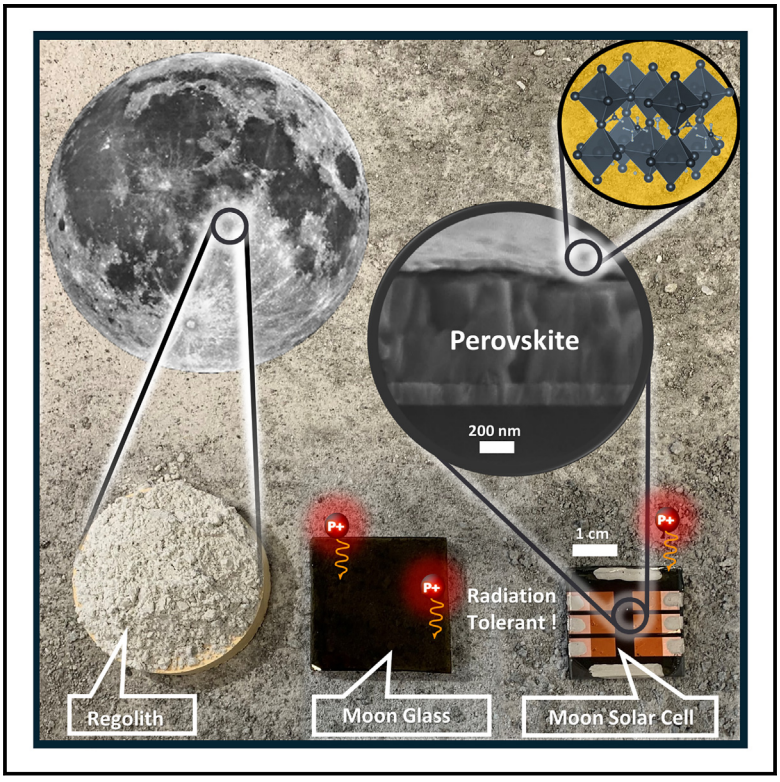

Highlights

- A novel strategy for Moon photovoltaics is proposed
- Combining abundant regolith with halide perovskites saves 99% of launch mass
- Enabling highest power-per-launched mass ratios with facile preparation on the Moon

Authors

Julián Mauricio Cuervo-Ortiz, Juan Carlos Ginés Palomares, Sercan Ozen, ..., Enrico Stoll, Stefan Linke, Felix Lang

Correspondence

felix.lang.1@uni-potsdam.de

In brief

This study proposes and fabricates perovskite-based Moon solar cells utilizing anorthositic regolith, an abundant resource on the Moon, to save ~99 wt % of required raw materials. This strategy enables power-per-launched mass ratios in excess of 22 W/g, a factor of 20–100 higher compared to traditional space PV solutions, to power future Moon settlements without compromising in radiation shielding, mechanical rigidity, and durability.

Cuervo-Ortiz et al., 2025, Device *3*, 100747
July 18, 2025
https://doi.org/10.1016/j.device.2025.100747

CellPress

Device

CellPress
OPEN ACCESS

Article

Moon photovoltaics utilizing lunar regolith and halide perovskites

Julián Mauricio Cuervo-Ortiz,[1,7] Juan Carlos Ginés Palomares,[2,7] Sercan Ozen,[1] Marlene Härtel,[3] Sema Sarisozen,[1] Alina Dittwald,[4] Georgios Kourkafas,[4] Andrés-Felipe Castro-Méndez,[1] Francisco Peña-Camargo,[1] Biruk Alebachew Seid,[1] Jürgen Bundesman,[4] Andrea Denker,[4,5] Heinz-Christoph Neitzert,[6] Dieter Neher,[1] Enrico Stoll,[2] Stefan Linke,[2] and Felix Lang[1,8,*]

[1]Institute of Physics and Astronomy, University of Potsdam, 14476 Potsdam-Golm, Germany
[2]Chair of Space Technology, Technische Universität Berlin, Marchstr. 12-14, 10587 Berlin, Germany
[3]Helmholtz-Zentrum Berlin für Materialien und Energie GmbH, und Energie GmbH, Photovoltaics Competence Centre Berlin (PVcomB), Schwarzschildstraße 3, 12489 Berlin, Germany
[4]Helmholtz-Zentrum Berlin für Materialien und Energie GmbH, und Energie GmbH, Protonen für die Therapie, 14109 Berlin, Germany
[5]Beuth Hochschule für Technik Berlin, Fachbereich II – Mathematik – Physik – Chemie, Luxemburgerstraße 10, 13353 Berlin, Germany
[6]Department of Industrial Engineering (DIIn), Salerno University, Fisciano, SA, Italy
[7]These authors contributed equally
[8]Lead contact
*Correspondence: felix.lang.1@uni-potsdam.de
https://doi.org/10.1016/j.device.2025.100747

THE BIGGER PICTURE Imagine a permanent moonbase, a village, or even a city on the Moon powered by the near-constant solar illumination at the lunar south pole. The problem: transporting enough conventional solar cells to the Moon, to supply lunar living, large habitats, research, construction, and first industrial activities. Here, we propose and demonstrate a novel solution that saves 99% of material transport weight and thus costs. Our approach utilizes the available regolith on the Moon to fabricate moonglass that serves as substrate and encapsulation to fabricate resilient moonglass/perovskite solar cells and modules. With ultrathin, defect-tolerant perovskite absorbers, this requires minimal material supply from Earth and is scalable to produce solar cells on the Moon with minimal equipment, resilient fabrication processes, and lowest energy payback times. Our hybrid approach outperforms strategies that rely on solar cells from Earth while avoiding complex and technology-intensive mining, extraction, and purification of semiconductors on the Moon. Being highly resilient to the harsh radiation environment, our moonglass/perovskite solar cells thus pave the way for sustainable lunar-energy solutions.

SUMMARY

Powering future Moon settlements requires reliable and cost-effective energy generation with high specific power. Here, we propose halide perovskite photovoltaics (PV) fabricated on regolith-based moonglass that could be produced on the Moon, thereby saving 99% of material transport weight. This enables effective specific power ratios, over 22–50 W/g, a factor of 20–100 higher compared to traditional space PV solutions, while not compromising radiation shielding, reliability, and mechanical stability as done until now. Using anorthosite high-glass-forming regolith simulant, we achieve transparent moonglasses that allow depositing high-quality perovskites. We achieve performances on par with references, revealing the potential of perovskite-based Moon photovoltaics, and propose routes to achieve power conversion efficiencies of 23%. The moonglass exhibits high tolerance to high-energetic proton irradiation, which, when combined with the radiation tolerance of perovskites, allows highly radiation-tolerant, reliable devices paving the way to future sustainable lunar-energy solutions.

INTRODUCTION

The closest celestial body to the Earth is the Moon, and, therefore, it is considered the first step for future sustainable space exploration with prolonged human presence, creating a sustainable and safe environment for humanity in space.[1,2] With the planned Lunar Gateway and crewed landings on the Moon in 2026 with Artemis 3, a permanent moonbase seems within

range. However, key technological advancements for lightweight, reliable, and cost-effective energy generation are imperative. Most planetary missions to date rely on solar cells for their power systems, primarily using III–V semiconductor-based multi-junction solar cells. These surpass 30% power conversion efficiency (PCE)[3,4] yet they provide specific powers of up to ~50/300 W/kg (cell/module level) only. This can be improved to ~200/1,000 W/kg (cell/module level) utilizing the newest roll-out-solar arrays in which the solar cell layer stack is epitaxially lift-off after production and adhered to a thin foil.[5,6] Recently, we and others proposed perovskite solar cells that could be manufactured directly on ultrathin foils (~10–200 μm), a cheaper and more scalable solution. The specific power of perovskite-based single and tandem solar cells can reach values of up to 1,000 W/kg, based on 100-μm thin substrate and encapsulation foils.[7] Yet these ultrathin foils provide little protection from radiation and micrometeorites and are prone to degrade in the harsh UV, atomic-oxygen (AtOx), radiation, and vacuum environment in space and on the Moon.[8] This dilemma between thick glass substrates/encapsulations offering radiation protection as well as mechanical stability vs. thin foils reducing launch mass is inevitably a delicate compromise, considering the exorbitant space transportation costs of about 1 million Euro/kg to the Moon.

Here, we propose using the lunar regolith, a layer of loose, homogeneous, and virtually inexhaustible material that blankets the crustal bedrock of the Moon, to overcome this compromise and dilemma. Our approach will enable solar cells with power-per-launched-mass ratios of up to 50,000 W/kg without sacrificing the advantages of millimeter-thick encapsulations offering mechanical and radiation protection for the underlying solar cells (calculation details in Tables S1, S3, S4, and Figure S2). For this purpose, we combine *in situ* resource utilized (ISRU) Moon regolith with ultrathin halide perovskite solar cells to fabricate efficient Moon-perovskite solar cells, as summarized in Figure 1. The first step is to fabricate moonglass of good optical quality, which can serve a dual purpose: as a substrate for perovskite solar cell fabrication and, being millimeter thick, as a protective cover for the harsh radiation environment on the Moon. Moreover, robust glass/glass encapsulated modules would allow easy handling and installation, similar to terrestrial applications, which would be extremely costly if millimeter-thick substrate/encapsulation needs to be sourced from Earth. Notably, the Moon regolith could be used without complex purification, and the equipment required can be as simple as a solar furnace. A solar furnace designed for lunar operations hereby would utilize parabolic mirrors or Fresnel lenses to concentrate sunlight into a highly focused area where the regolith is subsequently heated and melted in order to produce moonglass. This system would benefit from the high solar flux (~1,400 W/m^2) on the Moon without the atmospheric attenuation seen on Earth. Perovskite solar cells fabricated on top of the regolith-based moonglass require ultrathin absorber layers only (~500–800 nm), allowing the fabrication of 400-m^2 solar cells with just 1 kg of perovskite raw material brought from Earth.[9] With processing temperatures <150°C, halide perovskite-based solar cells offer lowest energy-payback times down to 0.15–0.40 years, compared to 1–2.5 years for silicon.[10–12] This is an important metric, considering that the energy required to build solar cells on the Moon must be produced on the Moon. Moreover, halide perovskites tolerate high impurity and defect concentrations in the 1%–10% range.[13] This will significantly facilitate future production on the Moon, allowing non-perfect deposition processes as well as a choice of various deposition techniques, ranging from printing to thermal evaporation or even a combination of the two in a sequential deposition. Halide perovskite-based solar cells have not only reached high efficiencies for single junctions of 25%[14] but their bandgap tunability also allows the fabrication of multi-junction solar cells,[15] offering future upgrades reaching efficiencies only achieved using expensive III–V semiconductor technologies. Lastly, halide perovskite single and tandem solar cells exhibit a unique radiation tolerance, making them ideal candidates for the extreme radiation environment on the Moon.[7,8,14,16] Assuming a small-scale production line with an equipment mass of around ~3 tonnes, producing moonglass/perovskite solar cells on the Moon would outperform solutions fabricated on Earth above a PV capacity of 3 MW, roughly capable of supplying a base for ~200 astronauts (extrapolating power requirements of the international space station [ISS]; see Figure S3).

Combining facile preparation on the Moon, utilizing a low quantity of high-quality raw materials sourced from Earth and an abundant resource on the Moon that can be used without complex purification steps, we believe our hybrid ISRU approach is highly realizable and easily scalable in the near future. Other proposed methods, which entirely rely on the mining of all raw materials on the Moon, require not only mining equipment but also metallurgical reduction methods, e.g., to reduce SiO_2 to silicon through molten regolith electrolysis, as well as various purification steps to provide semiconductor raw materials with low impurity concentration <ppb; see also our detailed comparison in Table S1. The high energy demand, together with more complex processing and fabrication techniques required, poses technological challenges on the Moon that likely will not be realizable in the near future, although advancements are being made.[19]

RESULTS AND DISCUSSION

Moonglass fabrication from TUBS-T regolith

Lunar regolith exhibits variations in composition and physical characteristics depending on whether it is found in the highlands (Terrae) or the lowlands (Maria) of the Moon. Regolith of the lunar highlands is mainly composed of anorthosite (a rock rich in calcium and aluminum), while regolith of the lunar lowlands are primarily composed of basaltic rocks (richer in iron and magnesium).[20] In this study, we primarily use the lunar regolith simulant TUBS-T, which is an anorthositic material produced at the Technische Universität Berlin that replicates the composition, mineralogy, and particle size distribution of the regolith found in highland terranes of the Moon.[21] TUBS-T, replicating anorthosite regolith, from highland terranes, is composed of 48.7 wt % SiO_2, 30.3 wt % Al_2O_3, 14.57 wt % CaO and contains low quantities of heavy metals oxides (with a low FeO and TiO_2 content of 1.05 wt % and 0.12 wt %, respectively), similar to lunar ferroan anorthosites that have been captured by the Apollo missions (see Table S1), making it a good glass former.[22] Basaltic regolith, replicated by the TUBS-M simulant, has a higher content of

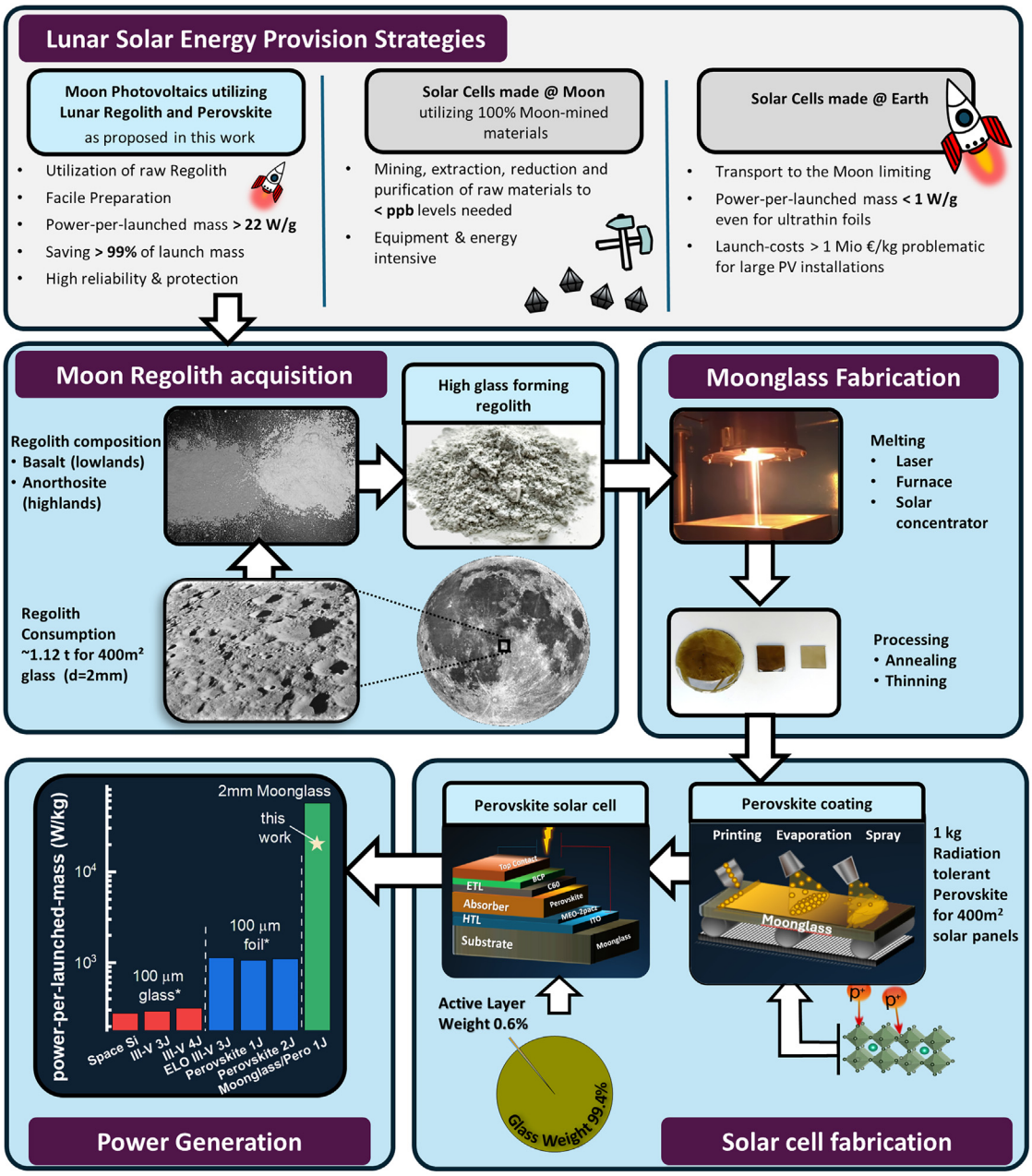

Figure 1. Overview over lunar solar energy provision strategies

Envisioned perovskite solar cell fabrication on the Moon, utilizing ISRU to produce moonglass from regolith, followed by halide perovskite solar cell deposition. 1 kg of perovskite precursors brought to the Moon, together with around 1.12 tons of regolith, are sufficient for around 400 m^2 of Moon-perovskite solar cells for a moonbase scenario like that presented by the ESA.[17] Also shown is the effective specific power, as power per launched mass, of the moonglass-based perovskite solar cells in comparison to traditional and recently proposed technologies. (Detailed calculations are summarized in the supplementary information.) For the moonglass fabrication panel, an extrusion of a regolith melt adapted from Stapperfend Berlin et al.[18] is shown.

heavy metals oxides (with a FeO content of 10.14 wt % and TiO_2 content of 2.29 wt %) and lower presence of Al_2O_3 and CaO (13.28 wt % and 8.31 wt %, respectively) in comparison to the TUBS-T.[21–23] In addition, MgO is also found in higher proportions in TUBS-M than in TUBS-T (8.73% against 0.57 wt %). These differences in chemical composition result in significant tonality differences between the simulants and the glasses manufactured with them[23] (see Figure 2A).

For the experiment validation in the laboratory, we fabricated moonglass by heating the powder at 1,550°C for 3 h in a platinum crucible inside a resistance furnace in vacuum followed by gradually cooling to room temperature to prevent damage of the

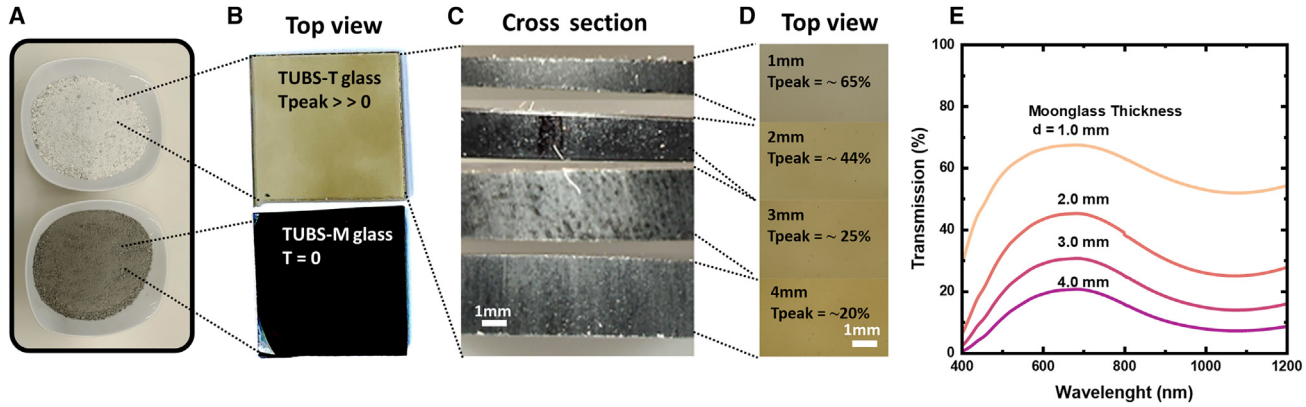

Figure 2. Regolith-based moonglass

(A and B) Photograph of TUBS-T and TUBS-M regolith simulants and glasses made thereof.

(C–E) Cross-sectional and top-view microscope images as well as transmission spectra of various thicknesses of TUBS-T moonglass.

glass due to thermal shock (for fabrication details see supplemental experimental procedures). Figure 2B displays top-view photographs of the resulting glass from both simulants. The TUBS-T glass exhibits good transparency compared to the TUBS-M, which exhibits no transparency. This is due to the chemical differences, especially the high FeO content of the lowland regolith simulated with TUBS-M. Hence, we selected highland regolith, simulated in TUBS-T for further solar cell fabrication, but note that the lowland regolith mimicked with TUBS-M could still be a good choice for the back glass of future glass/glass solar modules. Moreover, we note that reduced gravitational convection on the Moon may affect the mixing dynamics during melting and, consequently, solidification, indicating that extrapolating glass production from Earth to the Moon will require careful consideration. To maximize the transmission of the TUBS-T glass for use in solar cells, we varied the thickness from 4 to 1 mm (see Figure 2C). This allowed a peak transmission at 700 nm of up to 20% (4 mm), 25% (3 mm), 44% (2 mm), and 65% (1 mm); see top-view microscope images and transmission spectra in Figures 2D and 2E. This transmission window is perfectly aligned with the absorption of a ~1.5-eV-bandgap halide perovskite. However, the transmission of moonglass is still lower than the transmission of standard glass (typically 90% transmission), which is attributed to the presence of FeO (1.05% in TUBS-T compared to 0.08% in standard glass and 10.14 wt % in TUBS-M) imparting a darkening effect on the glass.

Halide perovskite deposition on moonglass

The formation of high-quality perovskite layers can strongly depend on the underlying substrate, its wettability and roughness, as well as its thermal expansion coefficients. In some cases, protonation reactions between the substrate (e.g., steel) and the perovskite are reported, which could diminish optoelectronic quality and lead to degradation.[13] In particular, the organic cations present in highly efficient perovskites, such as methylammonium (MA) and formamidinium (FA), are prone to react with some metal oxides that may be present in the Moon regolith (e.g., FeO, TiO_2, Al_2O_3, MgO, CaO, Na_2O, K_2O, MnO, Cr_2O_3).[13,21] Previous works developing perovskite on metal foils tackled this by inserting barrier layers such as 300-nm Ti or 100-nm indium-doped tin-oxide (ITO).[24] Nevertheless, the out-diffusion of glass impurities through these thin barriers into the semiconductor could potentially create trap states that lead to parasitic recombination. This is a severe problem for liquid-crystallized silicon on glass substrates, for which specialized glasses and multilayer barrier layers are required.[25] Moreover, high roughness requires the use of smoothing interlayers such as 5-μm polymers or time-consuming polishing steps to achieve high efficiencies.[26,27] On the contrary, Singh et al. recently revealed that some rout mean square (RMS) roughness at the order of 3.6-nm allows suppression of degradation compared to ultra-smooth surfaces at around 2-nm RMS.[28] Lastly, thermal expansion coefficients in the substrate that are vastly different from those of the perovskite semiconductor can lead to buildup of stress and microstrain of the perovskite, impairing performance and also leading to poor stability.[29] Again, this may require balancing interlayers for mitigation.

To assess the feasibility of fabricating perovskite solar cells on moonglass, we investigated the microstructural and optical properties of a $Cs_{0.05}(MA_{0.02}FA_{0.98})_{0.95}Pb(I_{0.98}Br_{0.02})_3$ triple-cation perovskite spin coated on top of a 2-mm thick moonglass. We employed this composition previously in inverted perovskite solar cells reaching efficiencies of over 23% (AM1.5G).[30,31] Prior to perovskite deposition, the moonglass was further coated with a 150-nm thin layer of indium-doped SnO_2 (ITO) as well as a thin self-assembling monolayer of Meo-2PACz, which serve as electrode and hole-transport layer later on, but we also investigated bare perovskite layers that were deposited directly onto the moonglass and do not find accelerated degradation behavior.

Figure 3A compares the morphology of perovskite films deposited on moonglass substrates and common glass, characterized with scanning electron microscopy (SEM). The top-view micrographs demonstrate nearly identical grain formation and spacing in the layers on both substrates (see also grain size distribution in Figure S3). Figure 3B presents grazing incidence wide-angle X-ray scattering (GIWAXS) diffractograms on both substrates conducted at an incident angle of 3° to reveal

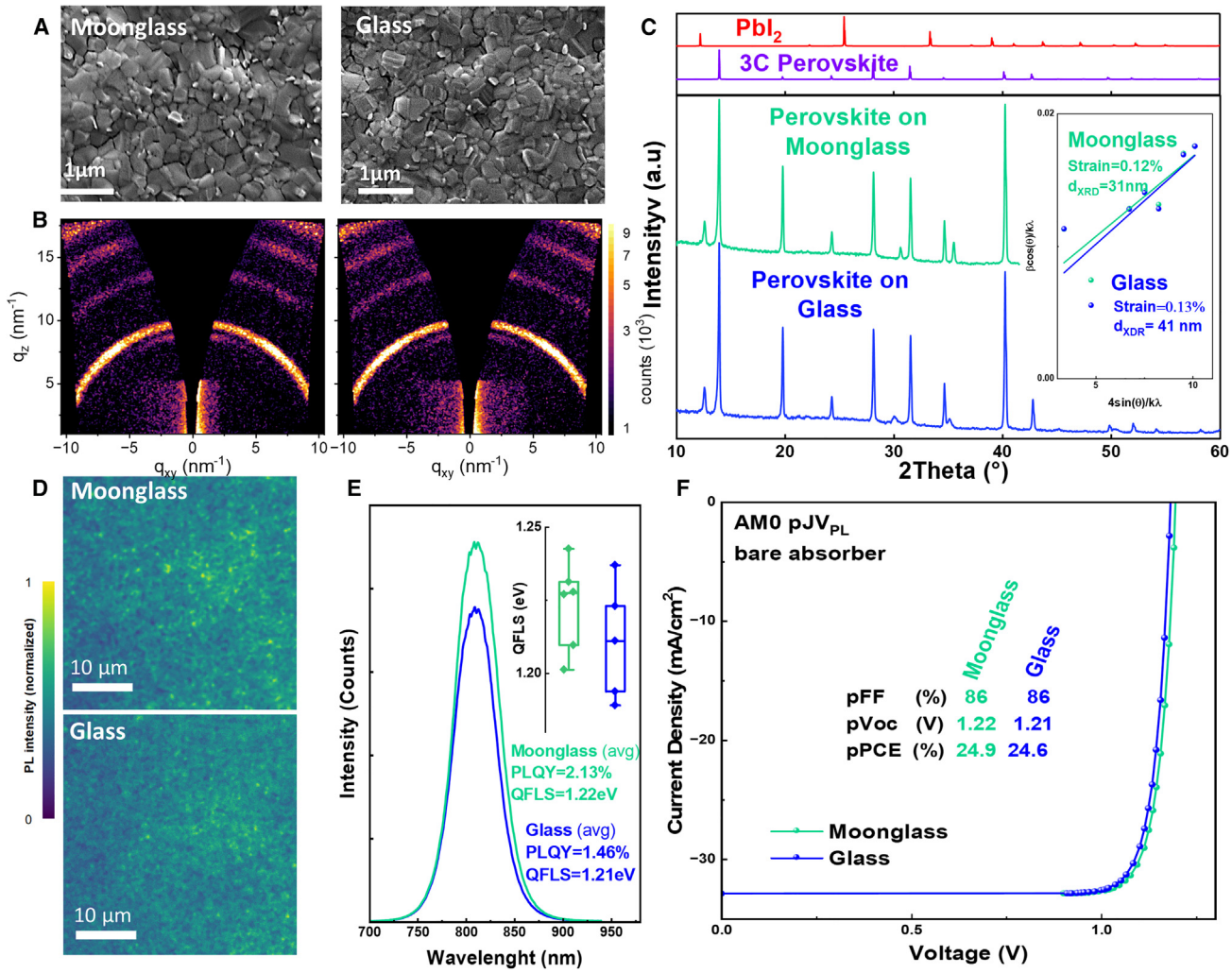

Figure 3. Perovskite on moonglass

(A) SEM top-view micrographs of perovskite films on moonglass and glass.

(B) GIWAXS for perovskite on moonglass and glass.

(C) XRD for PbI_2, triple-cation perovskite and crystallite size and strain comparison for moonglass and glass.

(D) PL images for neat perovskite layer on moonglass and glass substrates 100× increment with blue-light excitation.

(E) PLQY for neat perovskite on moonglass and glass with QFLS statistics calculated from PLQY measurements of various moonglass/glass samples. Box plots indicate 25-75% ranges and 1.5IQR whiskers.

(F) Pseudo-JV characteristics of bare perovskite absorbers on moonglass/glass from intensity-dependent PLQY measurements.

information on the texturing of the perovskite bulk. The results expose well-defined diffraction rings of the perovskite (e.g., at q = 0.99 Å^{-1}), indicative of a good polycrystallinity. Comparing GIWAXS results on glass and moonglass reveals an identical picture where intensity, position, and azimuthal behavior barely vary, indicating that the moonglass substrate does not induce further texturing of the perovskite (see also Figures S4 and S5). Further corroboration of these findings is provided by an X-ray diffraction (XRD) analysis in Figure 3C. The integrity of the perovskite on both substrates is well correlated with expected diffraction patterns without significant peak shifts that would indicate strain due to mismatched thermal expansion. In both films, we observe the presence of PbI_2 corresponding to the used PbI_2 excess in the perovskite precursor solution. We then utilized the Williamson Hall model (see inset in Figure 3C) to evaluate potential microstrain and find comparably low values for the perovskite layer on moonglass (0.13%) and on glass (0.12%) with slightly smaller crystallite sizes of 31 nm on the moonglass compared to 41nm on glass, indicating slightly denser nucleation. To probe the optoelectronic quality, we recorded photoluminescence (PL) images, photoluminescence spectra, and the photoluminescence quantum yield (PLQY) from the perovskite side (see Figures 3D and 3E, respectively). We find identical PL images and spectra but a slightly higher PLQY for moonglass at 2.1% compared to glass at 1.5% on average. We then recorded intensity-dependent PLQYs to calculate pseudo-current

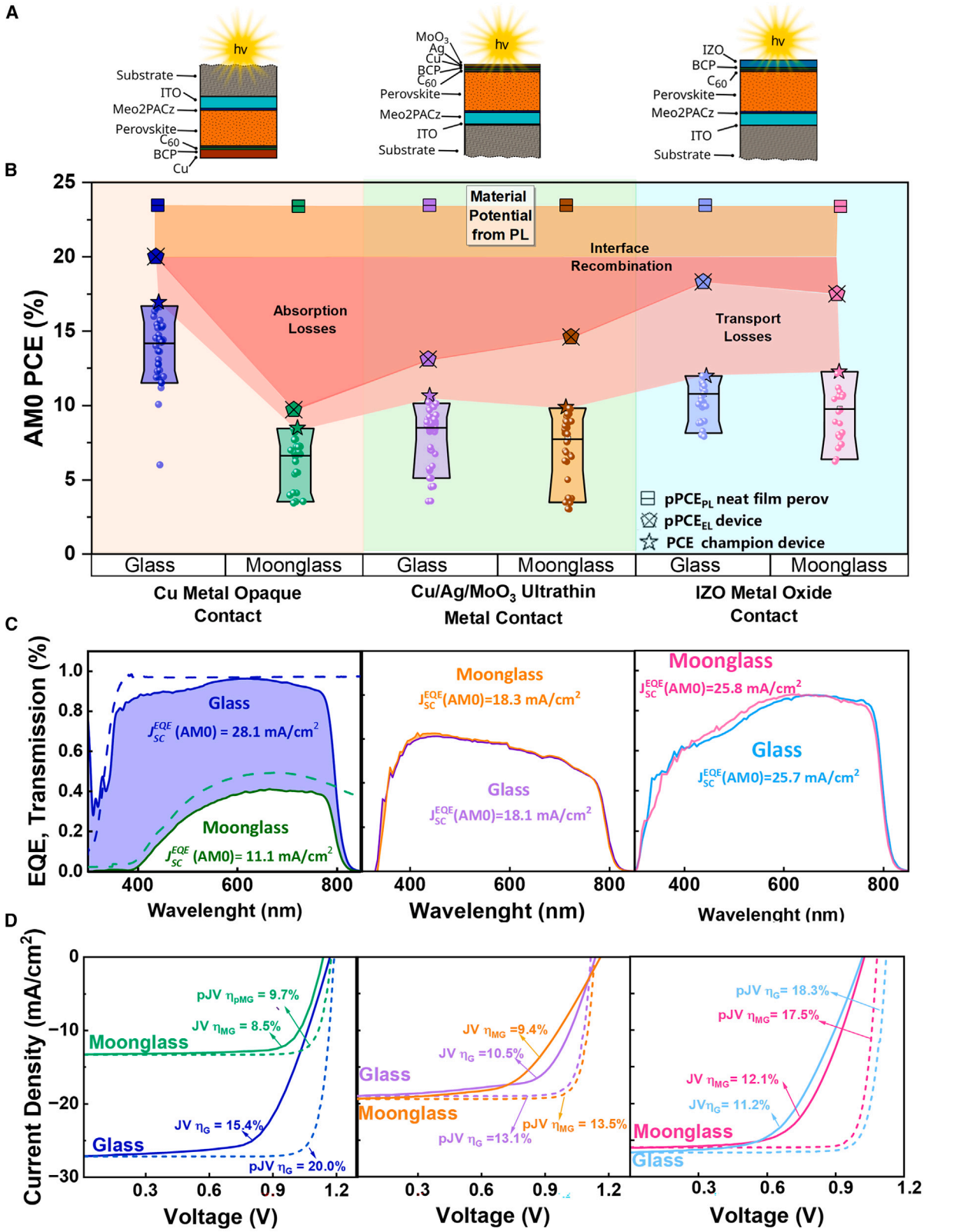

(legend on next page)

voltage (pJV_{PL}) characteristics, as shown in Figure 3F. As we described previously, these provide insights into the efficiency potential of the respective perovskite films based on their material quality.[32] Here, we find identical pseudo-fill-factors (pFFs) and pV_{OC}s as well as an efficiency potential of 24.9% and 24.6% on moonglass and normal glass, respectively. This reveals an optimal optoelectronic quality of the perovskite deposited on moonglass. We further find no impact of potential outdiffusion of impurities from the moonglass into the perovskite on performance and quality of devices even at long timescales (see Figure S8).

Moonglass-perovskite solar cells

Given the promising optical, morphological, and structural properties that perovskite deposition on moonglass exhibited, we introduced the 2-mm moonglass in a full perovskite single-junction solar cell utilizing a standard opaque p-i-n configuration using 100-nm layer of Cu as back electrode (superstrate configuration, Figure 4A). A detailed description of the device fabrication can be found in the supplemental experimental procedures. Control devices on glass substrates reached power conversion efficiencies (PCEs) of 18.6% and 16.4% under AM1.5G (100 mW/cm^2) and AM0 (136 mW/cm^2) illumination conditions, respectively (see Figures 4B and S9). This efficiency can be increased by using ITO layers with lower resistance (e.g., using commercial ITO-coated glass featuring 20 Ω^{-1} compared to 55 Ω^{-1} in our custom-made ITO), enabling PCEs of 20.2% (AM1.5G) and 17.1% (AM0) (see Figure S9). Moreover, passivation of the perovskite/C_{60} interface, e.g., using LiF, carborane, or 2D perovskites, as we have demonstrated previously,[30] would push the efficiencies further by up to +2% absolute, reaching 23.2% and 19.8% (AM0) (see Figure S9), yet this was not the focus of this paper.

The PCE of moonglass-based solar cells reached up to 8.5% (AM0), which sets a milestone for Moon-based perovskite solar cells yet is lower than the glass control devices. This difference can be primarily attributed to the dark pigmentation of the moonglass, which reduces the peak of light transmission (Tpeak) from ~95% to Tpeak = 44% for a thickness of d = 2 mm. This is reflected in a reduced external quantum efficiency (EQE) and short-circuit current (Jsc) from ~90% maximally and 28 mA/cm^2 (AM0, glass) to ~40% and 13 mA/cm^2 (see Figures 4B and 4C). To investigate the performance losses further, we recorded the electroluminescence (EL) quantum yield (ELQY) as a function of injection current. Similar to intensity-dependent PLQY measurements, this allowed us to extract pseudo-JV_{EL} (pJV_{EL}) characteristics that are free from series resistance effects. In both cases, we find a pFF_{EL} of ~88% and identical pV_{OC}s, highlighting the good perovskite deposition on moonglass. The pFF_{EL} is significantly higher than the FF of around 73%, indicating severe series resistance limitation from our custom-made ITO. Improving the ITO by optimizing deposition or post-deposition annealing would enable an increase in PCE, as seen in Figure 4D. Nonetheless, devices fabricated in the superstrate configuration will remain limited by the parasitic absorption of the moonglass.

To circumvent the parasitic absorption of the moonglass, we implemented a substrate configuration in which the perovskite solar cell is illuminated from the top contact side and not through the moonglass. For this purpose, we developed an ultrathin semitransparent metal contact comprising Cu (1 nm)/Ag (10 nm)/MoO_3 (20 nm) that can be thermally evaporated as well as a transparent conductive oxide contact that utilizes a sputtered indium zinc oxide (IZO) layer of 150 nm. A comparison of the respective device stacks is shown in Figure 4A, while full fabrication details, as well as optimization details, are given in the supplemental experimental procedures and Figure S13. Devices based on the ultrathin Cu/Ag/MoO_3 contact reached similar PCE, J_{SC}, and EQE values of ~10%, 18 mA/cm^2, and 63% on moonglass and glass (see Figures 4B and 4C), highlighting that the parasitic absorption of the moonglass was successfully circumvented. Although optimized Ag and MoO_3 thicknesses allowed the reflection and parasitic absorption of the ultrathin metal contact to be reduced down to record values compared with the literature,[33] the ultrathin Cu/Ag/MoO_3 contact layer still exhibits significant optical losses by itself. These optical losses were further reduced in devices utilizing IZO contacts, enabling even higher EQE and J_{SC} values of 88% and 26 mA/cm^2 both on moonglass and normal glass (see Figures 4B and 4C). Since no sputter buffer layer was used, the selected sputter process was a soft-sputter process, optimized for sensitive substrate layers.[34] This allowed improved efficiencies of 12.3% and 11.6% on the moonglass and glass, respectively. However, devices based on ultrathin Cu/Ag/MoO_3 and IZO are still limited by the sheet resistance of our custom-made ITO and semitransparent top contacts, which impacts the FF. Further optimization of these layers or the simple use of additional contact grids will further reduce transport losses and enable performances on par with pJV_{EL} to be reached, as shown in Figure 4D.

Another strategy to reduce the parasitic absorption of the moonglass is reducing its thickness. For the TUBS-T regolith-based moonglass, we simulate transparencies above 80% for d = 0.25 mm; see Figure 5A. Drift diffusion simulations, perfomed using the Simulation Software for Organic and Perovskite Solar Cells and LEDs (SETFOS)[35] as detailed in the supplementary information, predict an achievable Jsc of 30.1 mA/cm^2 (Figure S15), which results in a PCE of 21.5% for 0.1-mm moonglass under AM0 illumination; see Figure 5B. Optimizing transport layers and interfaces would further boost this efficiency to 22.1% and 22.7%, as $pPCE_{EL}$ and $pPCE_{PL}$ results suggest.

Our three designs utilizing opaque Cu, transparent ultrathin metal, or transparent IZO contacts demonstrate the feasibility

Figure 4. Perovskite-based solar cells on moonglass

(A) Layer stack for the different fabricated devices.

(B) PCE_{AM0} for perovskite on moonglass and glass with the Cu, Cu/Ag/MoO_3, and IZO top contacts. Also shown are their $pPCE_{el}$ measured on complete devices and the $pPCE_{pl}$ from neat films.Box plots indicate 10,25,75,90% ranges & mean lines.

(C) Corresponding EQE of champion devices with their integrated Jsc for the different substrate and top contact configurations.

(D) J-V(solid lines) and pJ-V_{el} curves (dashed lines) for the different substrate and top contact configurations.

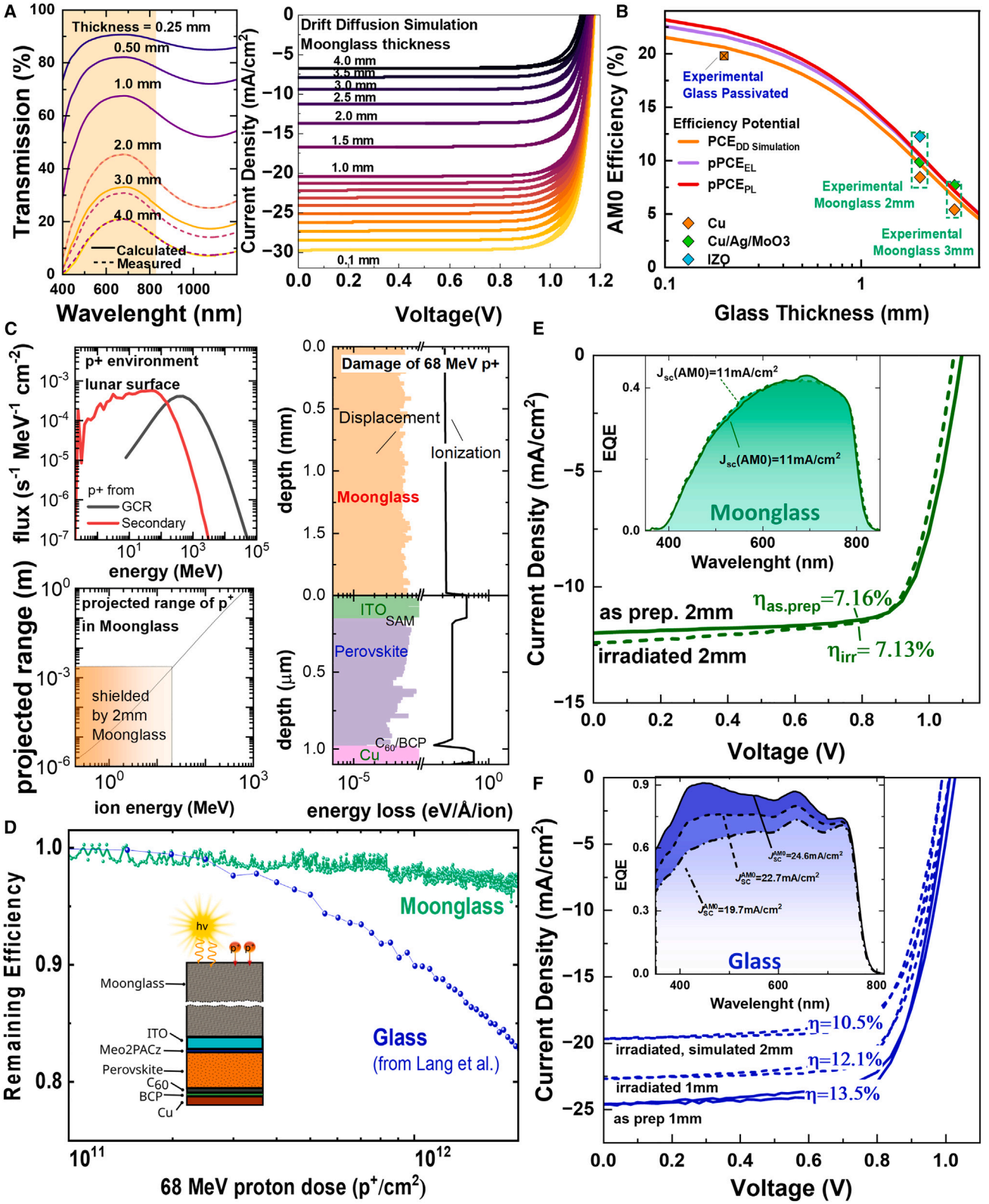

(legend on next page)

of highly efficient perovskite-based moonsolar cells, comparable with glass reference samples. For a first adoption, we believe that the most simple design using opaque metal electrodes will have advantages over the more complex ultrathin metal or IZO architectures. However, the transparent top contact design could be particularly relevant for regions on the Moon with higher FeO impurities, resulting in even darker moonglass, similar to the TUBS-M glass shown in Figure 2. Additionally, magnetic separation techniques, proposed by Schleppi et al.,[37] would enable a decrease in FeO impurity concentration, thereby improving moonglass transparency toward a transmission of 80%–90%. Magnetic separation promises a rather facile integration into future moonglass fabrication without the high purification demands needed for sourcing PV-grade silicon (∼ppb impurity levels) for silicon solar cell fabrication on the Moon.

Overall, our results pave the way for future moonsolar cells based on halide perovskites, an approach that, considering the facile perovskite and moonglass fabrication, outshines other proposed methods to produce solar cells on the Moon. Fabrication of silicon solar cells on the Moon from regolith has been proposed and discussed extensively since the 1990s.[38,39] However, the refinement of regolith to high-purity silicon for optoelectronics (impurity concentration <1 ppb) and the fabrication of silicon solar cells require highly complex processes. This makes fabricating efficient silicon solar cells on the Moon a highly complex endeavor. On Earth, high-purity silicon wafers, the starting material for silicon solar cells, are obtained by carbon arc welding of crushed quartz, reducing SiO_2 to CO_2 and molten silicon with 99% purity. Then, in a second step, the silicon is further purified via floating zone purification, and then finally (once impurities are <1 ppb), silicon ingots are made using Czochralski growth.[40] We believe these purification steps still pose tremendous technological challenges on the Moon, considering the impure regolith as the starting material. The required equipment likely will be significantly more complex compared to perovskite and moonglass fabrication, and, moreover, lower material quality/purity would impair efficiency significantly. Lastly, standard silicon solar cells are highly susceptible to radiation damage, which would accumulate in the harsh radiation environment of the Moon.[8]

Radiation tolerance

A crucial requirement for the adoption of moonglass-based solar cells on the Moon is their ability to resist the harsh radiation environment present. Compared with the radiation flux at the ISS, there is a significantly higher radiation flux on the Moon due to the solar and cosmic radiation but also a slowed-down/secondary radiation coming from high-energetic particles that hit the Moon regolith. Both are a threat for astronauts but also for the performance of solar cells/electronic components. Figure 5C shows the resulting proton radiation field.[36,41] In Figure 5C, we evaluate the shielding capabilities of the TUBS-M moonglass for high-energetic protons. Our Stopping and Range of Ions in Matter (SRIM) calculations reveal that a thickness of 2 mm is capable of shielding protons below ∼20 MeV, which constitute the majority of damage in thin-film solar cells. Typical coverglass thicknesses used in space are about 100 μm, while, due to the exorbitant transport costs, thicker shielding is rarely used. Nevertheless, even with 2-mm moonglass, higher energies are not blocked, and thus can still damage the underlying solar cell device stack. To evaluate the capability of our moonsolar cells to withstand the radiation spectrum on the Moon, we have therefore chosen a proton energy of 68 MeV, which mimics the expected damage profile due to a polyenergetic, omnidirection radiation spectrum, as present on the Moon, very well. Figure 5C shows the energy loss of 68 MeV p^+ in the Moonsolar cell-layer stack, revealing a homogeneous damage profile throughout the moonglass as well as the active layers of the perovskite solar cell. While we have previously developed halide perovskite single and tandem solar cells with the highest radiation tolerance,[7,8,14,16] most glass substrates darken significantly under radiation due to the formation of color centers in the glass. Without using specialized radiation-tolerant glasses, e.g., using high-purity quartz or adding CeO_2,[42] this can lead to a decrease in J_{SC} and thereby deteriorate the performance of solar cells. A crucial question is, therefore, whether the moonglass, with many pre-existing color centers, darkens further upon radiation exposure.

Figure 5D depicts the remaining efficiency of a 2-mm moonglass solar cell, measured during 68-MeV proton irradiation up to a total dose of $\phi = 2 \times 10^{12}$ $p^+ \cdot cm^{-2}$. Surprisingly, the moonglass-based device retained approximately 96% of its initial performance during the *in situ* experiment. To put this into context, we plotted previous *in situ* measurements of an $MAPbI_3$ solar cell on 1-mm glass alongside Figure 5D, revealing a remaining factor of only 82%, partly from glass coloring and partly from radiation damage in the perovskite that later self-healed (see Lang et al.[16]). Post-irradiation measurements of the moonglass solar cell, conducted 3 weeks after the irradiation once the remaining activity allowed safe handling, revealed an identical EQE and only a reduction of PCE of $0.03\%_{abs}$. This indicates a post-irradiation remaining factor of 0.996 (see Figure 5E) and implies no deterioration of the moonglass or the

Figure 5. Stability of moonglass-based perovskite solar cells and efficiency potential

(A) Calculated transmission and simulated JV characteristics for different TUBS-T regolith-based moonglass thicknesses.

(B) Simulated PCE_{AM0} from a coupled drift-diffusion and optics simulation in SETFOS as a function of moonglass thicknesses alongside experimental results and PCE potentials from pseudo-JV characteristics derived from EL and PL.

(C) Albedo particle flux of the Moon, showing protons from the galactic cosmic radiations as well as secondary protons induced by the lunar soil. Neutrons, positrons, electrons, and gamma rays are not shown. Data adapted from Dobynde et al.[36] SRIM simulation of the projected range of high-energetic protons in moonglass showing the shielding capability of, e.g., 2-mm moonglass. SRIM simulation of the damage profile under 68 MeV p+, revealing a homogeneous damage profile within the moonglass and the perovskite solar cell, similar to what is expected from omnidirectional, polyenergetic radiation environment.[8]

(D) Remaining efficiency of perovskite solar cells on 2-mm moonglass and 1-mm standard glass under 68-MeV proton irradiation up to a proton dose of 2E12 p^+/cm^2.

(E and F) Measured JV parameters before and after proton radiation for perovskite devices on 2-mm moonglass, 1-mm standard glass, and estimated results for 2-mm standard glass.

perovskite. To put these results into context, we extrapolated post-irradiation results of an $FA_{0.7}Cs_{0.3}Pb(I_{0.9}Br_{0.1})_3$ based p-i-n solar cell on 1-mm glass from Lang et al.[14] to AM0 conditions in Figure 5F, and we found a remaining factor of 0.88 in the case of a 1-mm standard-glass substrate due to glass coloring leading to a reduced EQE and predict a remaining factor of 0.79 for a 2-mm glass substrate.

In comparison, the TUBS-T moonglass therefore exhibits a surprising radiation tolerance on par with expensive Ce-doped glasses. Formation of color centers in conventional amorphous glasses upon ionizing radiation is ultimately due to the ionization and subsequent electron and hole trapping, e.g., at an F center. Cerium, featuring Ce^{3+}/Ce^{4+} oxidation states in glass, allows acceptance of electron/holes, respectively, thus preventing the formation of color centers. Our typical moonglass contains about 1% of iron, which also exhibits Fe^{2+}/Fe^{3+} charge states. This iron impurity can suppress formation of trapped electron/hole color centers similar to cerium[43,44] and consequently can protect the moonglass from radiation-induced coloring. This extraordinary radiation tolerance of TUBS-T moonglass, mimicking raw anorthositic regolith found in highland terranes, together with the radiation tolerance of halide perovskites, is a crucial factor for future long-term-stable Moon solar cells that survive the most extreme radiation conditions.

Conclusions

In conclusion, we have set the first foundation for future solar cells that can be produced on the Moon. We demonstrated that utilizing raw anorthositic regolith found in highland terranes of the Moon as transparent moonglass substrate and encapsulation, together with halide perovskites thin-film solar cells, has the potential to provide the highest power-to-launched-mass ratios of ~22–50 W/g while not sacrificing thick encapsulation solutions for radiation shielding, reliability, and mechanical stability or relying on complex mining, extraction, and purification techniques. We proposed and tested three device configurations utilizing opaque Cu electrodes in a superstrate configuration as well as transparent ultrathin metal and IZO designs in substrate configurations. In the substrate configurations, PCEs reached 9.4% (with the ultrathin metal contact) and 12.1% (with IZO) on moonglass under unoptimized conditions for the deposition of the contact layers, comparable to efficiencies achieved on normal glass substrates. Further optimization of the transparent contact layers to reduce the series resistance of the devices could allow a PCE of 17.5%, as suggested by the pJV_{EL} measurements. On the other hand, using the simpler superstrate configuration with opaque electrodes, moonglass-based devices reached a PCE of 8.6%, limited by the parasitic absorption of the 2-mm thick moonglass. This could be circumvented using thinner moonglasses, and we predict efficiencies of ~21% that can be reached by using 0.1-mm glass and interface passivation. Experiments under high-energetic proton irradiation further revealed high radiation tolerance of the anorthositic regolith-based moonglass to radiation-induced coloring. This enabled highly radiation-tolerant moonglass-based perovskite solar cells that retain 99.6% of their initial efficiency after exposure to 2×10^{12} 68 MeV $p^+ \cdot cm^{-2}$. Combining high radiation tolerance, highest power-per-launched-mass ratios, and a facile fabrication, our regolith-based Moon-perovskite solar cells are the most promising route to power future Moon habitats in the near future.

METHODS

Full details of experimental procedures can be found in the supplemental information.

RESOURCE AVAILABILITY

Lead contact

Further information and requests for resources should be directed to the lead contact, Dr. Felix Lang (felix.lang.1@uni-potsdam.de).

Materials availability

Materials and methods are described in the section "experimental procedures" in the supplemental information.

Data and code availability

All data of this study are available within the article or the supplemental information.

ACKNOWLEDGMENTS

F.L. acknowledges the Volkswagen Foundation for funding via the Freigeist Program.

AUTHOR CONTRIBUTIONS

J.M.C.O. fabricated, optimized, and analyzed the moonglass-based perovskite solar cells. J.C.G.P. fabricated the moonglass. S.O. conducted and analyzed the GIWAXS results. M.H. deposited the ITO and IZO. S.S. conducted the SEM imaging and XRD. A.F.C.-M. and F.P.C. helped interpret and analyze the results. B.A.S. helped interpret and analyze the results and optimized perovskite solar cells. H-C.N., A.Dittwald., G.K., J.B., and A.Denker. performed the proton irradiation experiments. S.L. and F.L. initiated the research and planned the experiments. All authors contributed to the discussion of the results. J.M.C.O., J.C.G.P., and F.L. took the lead in drafting the manuscript with input from all co-authors.

DECLARATION OF INTERESTS

The authors declare no competing interests.

SUPPLEMENTAL INFORMATION

Supplemental information can be found online at https://doi.org/10.1016/j.device.2025.100747.

Received: December 9, 2024
Revised: February 12, 2025
Accepted: February 21, 2025
Published: April 3, 2025

REFERENCES

1. Vaccaro, H., and Castillo, T. (2023). Gateway Program Safety and Mission Assurance Integration - The Future of Safe Deep Space Human Exploration. https://ntrs.nasa.gov/api/citations/20220018504/downloads/12th-IAASS-conference-abstract-Gateway-SMA_tree.doc.pdf.
2. o.V (2020). NASA's Lunar Exploration Program Overview (Nasa).
3. Li, J., Aierken, A., Liu, Y., Zhuang, Y., Yang, X., Mo, J.H., Fan, R.K., Chen, Q.Y., Zhang, S.Y., Huang, Y.M., and Zhang, Q. (2021). A Brief Review of High Efficiency III-V Solar Cells for Space Application. Front. Phys. *8*, 1–15. https://doi.org/10.3389/fphy.2020.631925.

4. Geisz, J.F., France, R.M., Schulte, K.L., Steiner, M.A., Norman, A.G., Guthrey, H.L., Young, M.R., Song, T., and Moriarty, T. (2020). Six-junction III–V solar cells with 47.1% conversion efficiency under 143 Suns concentration. Nat. Energy *5*, 326–335. https://doi.org/10.1038/s41560-020-0598-5.

5. Banik, J., Kiefer, S., LaPointe, M., LaCorte, P., and Drive, W. (2018). On-orbit validation of the roll-out solar array. In 2018 IEEE Aerospace Conference (IEEE) (IEEE), pp. 1–9. https://doi.org/10.1109/AERO.2018.8396390.

6. Hoang, B., Way, F., Alto, P., Hoangsslmdacom, B., White, S., Space, D., Dss, S., Drive, W., Suite, F., Barbara, S., et al. (2016). Commercialization of Deployable Space Systems' Roll-Out Solar Array (ROSA) Technology for Space Systems Loral (SSL) Solar Arrays, *1–12*.

7. Lang, F., Eperon, G.E., Frohna, K., Tennyson, E.M., Al-Ashouri, A., Kourkafas, G., Bundesmann, J., Denker, A., West, K.G., Hirst, L.C., et al. (2021). Proton-Radiation Tolerant All-Perovskite Multijunction Solar Cells. Adv. Energy Mater. *11*, 2102246. https://doi.org/10.1002/aenm.202102246.

8. Lang, F., Jošt, M., Frohna, K., Köhnen, E., Al-Ashouri, A., Bowman, A.R., Bertram, T., Morales-Vilches, A.B., Koushik, D., Tennyson, E.M., et al. (2020). Proton Radiation Hardness of Perovskite Tandem Photovoltaics. Joule *4*, 1054–1069. https://doi.org/10.1016/j.joule.2020.03.006.

9. McMillon-Brown, L., Luther, J.M., and Peshek, T.J. (2022). What Would It Take to Manufacture Perovskite Solar Cells in Space? ACS Energy Lett. *7*, 1040–1042. https://doi.org/10.1021/acsenergylett.2c00276.

10. Celik, I., Song, Z., Cimaroli, A.J., Yan, Y., Heben, M.J., and Apul, D. (2016). Life Cycle Assessment (LCA) of perovskite PV cells projected from lab to fab. Sol. Energy Mater. Sol. Cells *156*, 157–169. https://doi.org/10.1016/j.solmat.2016.04.037.

11. Celik, I., Philips, A.B., Song, Z., Yan, Y., Ellingson, R.J., Heben, M.J., and Apul, D. (2018). Energy payback time (EPBT) and energy return on energy invested (EROI) of perovskite tandem photovoltaic solar cells. IEEE J. Photovoltaics *8*, 305–309. https://doi.org/10.1109/JPHOTOV.2017.2768961.

12. Gong, J., Darling, S.B., and You, F. (2015). Perovskite photovoltaics: life-cycle assessment of energy and environmental impacts. Energy Environ. Sci. *8*, 1953–1968. https://doi.org/10.1039/C5EE00615E.

13. Liu, C., Wu, W., Zhang, D., Li, Z., Ren, G., Han, W., and Guo, W. (2021). Effective stability enhancement in ZnO-based perovskite solar cells by MACl modification. J. Mater. Chem. A *9*, 12161–12168. https://doi.org/10.1039/D1TA02697F.

14. Lang, F., Chiang, Y.-H., Frohna, K., Ozen, S., Neitzert, H.C., Denker, A., Stolterfoht, M., and Stranks, S.D. (2023). Methylammonium-free co-evaporated perovskite absorbers with high radiation and UV tolerance: an option for in-space manufacturing of space-PV? RSC Adv. *13*, 21138–21145. https://doi.org/10.1039/D3RA03846G.

15. Best Research-Cell Efficiencies. (2024). https://www.nrel.gov/pv/cell-efficiency.html.

16. Lang, F., Nickel, N.H., Bundesmann, J., Seidel, S., Denker, A., Albrecht, S., Brus, V.V., Rappich, J., Rech, B., Landi, G., and Neitzert, H.C. (2016). Radiation Hardness and Self-Healing of Perovskite Solar Cells. Adv. Mater. *28*, 8726–8731. https://doi.org/10.1002/adma.201603326.

17. ESA - Artist impression of activities in a Moon Base. Available at: https://www.esa.int/ESA_Multimedia/Images/2019/07/Artist_impression_of_activities_in_a_Moon_Base.

18. Stapperfend Berlin, S.T., Stefan Linke Berlin, G.T., Kai-Uwe Hess, G., and Bruce Dingwell, D. (2023). Additive manufacturing with Molten Lunar Regolith under Vacuum Conditions. In 74th International Astronautical Congress 2023 IAF MATERIALS and STRUCTURES SYMPOSIUM (C2) Space Structures II-Development and Verification (Deployable and Dimensionally Stable Structures) (2).

19. Blue Alchemist. (2025). https://ntrs.nasa.gov/api/citations/20060004126/downloads/20060004126.pdf.

20. Crawford, I.A. (2015). Lunar resources: A review. Prog. Phys. Geogr. Earth Environ. *39*, 137–167. https://doi.org/10.1177/0309133314567585.

21. Linke, S., Windisch, L., Kueter, N., Wanvik, J.E., Voss, A., Stoll, E., Schilde, C., and Kwade, A. (2020). TUBS-M and TUBS-T based modular Regolith Simulant System for the support of lunar ISRU activities. Planet. Space. Sci. *180*, 104747. https://doi.org/10.1016/j.pss.2019.104747.

22. Windisch, L., Linke, S., Jütte, M., Baasch, J., Kwade, A., Stoll, E., and Schilde, C. (2022). Geotechnical and Shear Behavior of Novel Lunar Regolith Simulants TUBS-M, TUBS-T, and TUBS-I. Materials *15*. https://doi.org/10.3390/ma15238561.

23. Harizanova, R., Mihailova, I., Cherkezova-Zheleva, Z., Paneva, D., Georgieva, M., Tzankov, D., Avdeev, G., and Rüssel, C. (2024). Glass–crystalline materials with high iron oxide concentration: Phase composition, redox ratio and magnetic properties. Boletín la Soc. Española Cerámica y Vidr *63*, 23–32. https://doi.org/10.1016/j.bsecv.2023.04.001.

24. Zhou, C., Xu, Y., Li, Y., Du, K., Li, X., Dong, X., Li, L., Yuan, N., and Ding, J. (2024). Flexible Perovskite Solar Cells on Ultra-Thin Stainless-Steel with a Power-to-Weight Ratio over 3000 W kg− 1. Sol. RRL *8*. https://doi.org/10.1002/solr.202300901.

25. Gabriel, O., Frijnts, T., Preissler, N., Amkreutz, D., Calnan, S., Ring, S., Stannowski, B., Rech, B., and Schlatmann, R. (2016). Crystalline silicon on glass—interface passivation and absorber material quality. Progress in Photovoltaics. *24*, 1499–1512. https://doi.org/10.1002/pip.2707.

26. Feleki, B.T., Bouwer, R.K.M., Wienk, M.M., and Janssen, R.A.J. (2022). Perovskite Solar Cells on Polymer-Coated Smooth and Rough Steel Substrates. Sol. RRL *6*. https://doi.org/10.1002/solr.202100898.

27. Kumar, A., Rani, S., and Sundar Ghosh, D. (2024). Kitchen-grade aluminium foil as dual-purpose substrate-cum-electrode for ultrathin, ultralight, and bendable perovskite solar cells. Sol. Energy Mater. Sol. Cells *268*, 112737. https://doi.org/10.1016/j.solmat.2024.112737.

28. Singh, S., Siliavka, E., Löffler, M., and Vaynzof, Y. (2024). Impact of Buried Interface Texture on Compositional Stratification and Ion Migration in Perovskite Solar Cells. Adv. Funct. Mater. *34*, 2402655. https://doi.org/10.1002/adfm.202402655.

29. Xue, D.J., Hou, Y., Liu, S.C., Wei, M., Chen, B., Huang, Z., Li, Z., Sun, B., Proppe, A.H., Dong, Y., et al. (2020). Regulating strain in perovskite thin films through charge-transport layers. Nat. Commun. *11*, 1514. https://doi.org/10.1038/s41467-020-15338-1.

30. Seid, B.A., Sarisozen, S., Peña-Camargo, F., Ozen, S., Gutierrez-Partida, E., Solano, E., Steele, J.A., Stolterfoht, M., Neher, D., Lang, F., et al. (2024). Understanding and Mitigating Atomic Oxygen-Induced Degradation of Perovskite Solar Cells for Near-Earth Space Applications. Small *20*, 2311097. https://doi.org/10.1002/smll.202311097.

31. Ye, F., Zhang, S., Warby, J., Wu, J., Gutierrez-Partida, E., Lang, F., Shah, S., Saglamkaya, E., Sun, B., Zu, F., et al. (2022). Overcoming C60-induced interfacial recombination in inverted perovskite solar cells by electron-transporting carborane. Nat. Commun. *13*, 7454. https://doi.org/10.1038/s41467-022-34203-x.

32. Lang, F., Köhnen, E., Warby, J., Xu, K., Grischek, M., Wagner, P., Neher, D., Korte, L., Albrecht, S., and Stolterfoht, M. (2021). Revealing Fundamental Efficiency Limits of Monolithic Perovskite/Silicon Tandem Photovoltaics through Subcell Characterization. ACS Energy Lett. *6*, 3982–3991. https://doi.org/10.1021/acsenergylett.1c01783.

33. Liu, H., Lang, R., Jiang, S., Lu, W., Zhang, W., Feng, L., Liu, H., Wu, L., Liu, X., Wang, X., and Yu, W. (2021). Bifacial semitransparent perovskite solar cells with MoOx/Cu/Ag/MoOx multilayer transparent electrode. Sol. Energy *228*, 290–298. https://doi.org/10.1016/j.solener.2021.09.065.

34. Härtel, M., Li, B., Mariotti, S., Wagner, P., Ruske, F., Albrecht, S., and Szyszka, B. (2023). Reducing sputter damage-induced recombination losses during deposition of the transparent front-electrode for monolithic perovskite/silicon tandem solar cells. Sol. Energy Mater. Sol. Cells *252*, 112180. https://doi.org/10.1016/j.solmat.2023.112180.

35. (2025). Semiconducting Thin Film Optics Simulator (SETFOS) by Fluxim AG, Switzerland. Available online: http://www.fluxim.com (accessed on 27. March 2025).

36. Dobynde, M.I., and Guo, J. (2021). Radiation Environment at the Surface and Subsurface of the Moon: Model Development and Validation. JGR. Planets *126*, e2021JE006930. https://doi.org/10.1029/2021JE006930.

37. Schleppi, J., Bromiley, G., Odling, N., and Bennett, N.S. (2021). In-situ resource utilisation manufacturing of optically transparent glass from lunar regolith simulant. J. Mater. Sci. *56*, 12132–12153. https://doi.org/10.1007/s10853-021-06059-x.

38. Ignatiev, A., Freundlich, A., Duke, M., and Rosenberg, S. (2002). The fabrication of silicon solar cells on the moon using in-situ resources. In 40th AIAA Aerosp. Sci. Meet. Exhib, p. 465. https://doi.org/10.2514/6.2002-465.

39. Sparks, D.R., Div, D.E., and Corp, G.M. (1987). The large-scale m a n u facturing of electronic and electrical components in space. Acta. Astronaut. *15*, 239–244.

40. Zulehner, W. (1983). Czochralski growth of silicon. J. Cryst. Growth. *65*, 189–213. https://doi.org/10.1016/0022-0248(83)90051-9.

41. Reitz, G., Berger, T., and Matthiae, D. (2012). Radiation exposure in the moon environment. Planet. Space Sci. *74*, 78–83. https://doi.org/10.1016/j.pss.2012.07.014.

42. Haynes, G.A. (1970). Effect of Radiation on Cerium-Doped Solar Cell Cover Glass. 6024, National Aeronautics and Space Administration.

43. SAKKA, S. Radiation-Induced Color Centers in Glasses. Bull. Inst. Chem. Res., Kyoto Univ., 48.

44. KREIDL, N.J., and HENSLER, J.R. (1955). Formation of Color Centers in Glasses Exposed to Gamma Radiation. J. Am. Ceram. Soc. *38*, 423–432. https://doi.org/10.1111/j.1151-2916.1955.tb14568.x.